Radar Classification of Human Gait Abnormality Based on Sum-of-Harmonics Analysis

Ann-Kathrin Seifert, Abdelhak M. Zoubir
Signal Processing Group
Technische Universität Darmstadt, 64283 Darmstadt, Germany
Email: {seifert, zoubir}@spg.tu-darmstadt.de

Moeness G. Amin
Center for Advanced Communications
Villanova University, Villanova, PA 19085 USA
Email: moeness.amin@villanova.edu

***Abstract*—Radar technology for monitoring of human gait has recently gained interest in the fields of home security, medical diagnosis, assisted living and rehabilitation. Due to its remote, reliable and privacy-preserving sensing, radar is promising to become an effective tool for medical gait analysis. We show the influences of gait abnormalities and assistive walking devices on the joint-variable representations of the back-scattered radar signals. Using both, parametric and non-parametric techniques, we extract gait features to classify normal, abnormal and cane-assisted gait. In particular, the fundamental frequency of the time-frequency behavior is estimated using sum-of-harmonics modeling in order to characterize different gaits. Results obtained using experimental K-band radar data are presented for the person-specific and person-generic case.**

I. Introduction

The human gait is a complex motion and requires the concerted interaction between many systems, including strength, sensation and coordination [1]. Deviations from a normal walk, which are generally referred to as gait abnormalities, provide information about a person's neurological, musculoskeletal and medical condition [2]. Observing a patient's gait plays a key role in many medical examinations. For example, different neurological conditions lead to very characteristic gaits [3]. Thus, the human gait can serve as an early indicator of several disorders.

Contrary to extensive clinical gait studies, we seek a cost-effective and efficient technology to collect and interpret gait data accurately and in realtime. Electromagnetic sensing for indoor human monitoring has become a key technology in home security, elderly care, and medical diagnosis applications [4], [5]. In contrast to other non-wearable sensing modalities such as infrared reflective light, video cameras, and in-ground force platforms [6], [7], radar is insensitive to lighting, can penetrate through common materials, preserves privacy and its performance is not impaired by clothing. Clearly, gait monitoring systems should not be affected by the use of assistive walking devices, such as a cane or crutches, which are commonly used by the elderly population aged over 65 years to gain mobility [8] and by patients in rehabilitation to reestablish a normal gait, respectively.

We show that radar signals of human walks contain detailed information on a person's gait. In particular, the time-frequency features that arise due to the micro-Doppler (mD) effect [9] are examined. By giving a detailed biomechanical interpretation of the observed mD signatures, we further the understanding of the state of gait normality and abnormality, which enhances the practitioners' ability for rendering diagnosis.

Human gait has previously been studied using radar in, e.g., [10], [11], [12]. However, radar-based human gait analysis and detection of walking aids has not been widely investigated so far [13], [14], [15], [16]. Opposed to existing radar-based human gait classification methods, which consider walks with and without arm swinging [17], [18], [19], [20], or different speeds of walking [21], [22], we focus on detecting differences in the lower limbs kinematics, i.e., all test subject were asked to walk slowly without arm swinging. In particular, we consider five different gaits including abnormal and cane-assisted walks, where the latter are motivated by the cane's widespread use and rising interest in the corresponding Doppler signatures [4], [23], [24], [16]. As such, we deal with an intra motion category classification problem, i.e., we distinguish different walking styles within the class of human gait.

For classifying normal, pathological and assisted gait, we use predefined features from the time-frequency representation (TFR) of the radar return signal. First, we describe the differences of the mD signatures in their TFR for different walking styles. Then, we proceed to model this time-frequency behavior as a sum-of-harmonics (SOH) to estimate the underlying fundamental frequency (FF) of the gait, which is used to calculate a descriptive feature for gait recognition. Using only a small number of features, we can reliably classify the considered gait classes. Results will be presented and discussed for the person-specific and person-generic case.

The remainder of this paper is organized as follows. Section II introduces TFRs of radar return signals of different human gaits and gives a biomechanical interpretation of the observed mD signatures. From these TFRs, features are extracted for classification of normal, abnormal and cane-assisted walking styles as described in Section III. Experimental results using real radar data are presented in Section IV and final conclusions are given in Section V.

II. Micro-Doppler signatures of human gait

A. Time-Frequency Representations

The highly non-stationary and multi-component back-scattered radar signal from a walking person is typically analyzed in joint-variable domains such as TFRs. The latter clearly reveal the time-varying mD features of a human gait in the joint Doppler frequency vs. time domain. This domain reveals the velocity, acceleration, and higher-order motion

978-1-5386-4167-5/18/$31.00 ©2018 IEEE

terms of the different parts of the human body. A typical choice of TFR for this application is the spectrogram [25]. For a discrete-time signal $s(n)$ of length N, the spectrogram is given by the squared magnitude of the short-time Fourier transform (STFT) [26]

$$\mathrm{S}(n,k) = \left| \sum_{m=0}^{L-1} w(m) s(n+m) \exp\left(-j2\pi \frac{mk}{K}\right) \right|^2, \quad (1)$$

for $n = 0, \ldots, N-1$, where L is the length of the smoothing window $w(\cdot)$, k is the discrete frequency index with $k = 0, \ldots, K-1$, and $L, K \in \mathbb{N}$.

Fig. 1 shows examples of spectrograms for different human walks, i.e., normal walking, limping with one and both legs, and walking with a cane. For the latter, we consider two different ways of using the cane: having the cane moved in alignment with one of the legs, and moving the cane out of sync with any leg. Further, we evaluate all walking styles for motions toward and away from the radar system.

The spectrogram of a typical normal gait when a person is walking toward the radar system is depicted in (a). The torso's motion can be identified by the highest energy due to its large radar cross section and consequently strongest reflections. The torso's time-frequency signature periodically varies between approximately 20 Hz and 110 Hz Doppler frequency, representing the acceleration and deceleration phases during the human walking cycle [9]. The time-frequency signature of the swinging foot shows a clear sinusoidal shape with up to about 300 Hz Doppler shift in this case. This mD signature, see e.g. in the time interval between 0 s and 1 s in (a), shall be referred to as stride signature below. In this case, the spectrogram reveals six stride signatures during the 6 s measurement. Note that there is no arm swinging involved in this motion.

In contrast to (a), the mD signature of a person walking away from the radar system is shown in (b). Here, we observe five strides in the 6 s measurement. The mD stride signatures are clearly different compared to the toward-radar measurement. For a detailed analysis of a human walk that is observed with a radar from behind see [24].

Figs. 1(c) and (d) show the spectrograms of a person walking with a limp toward and away from the radar system, respectively. Here, limping refers to the inability to bend one of the knees properly. Thus, every other stride signature in (c) and (d) is different from that of a normal stride. That is, in the toward-radar case, the second, forth and sixth mD signatures are due to a limping leg, where in the away-from-radar measurement the first, third, fifth and seventh stride signatures are abnormal. For both measurements, we observe that the abnormal stride signatures have a smaller maximum Doppler shift compared to a normal stride signature. Further, due to the straight leg's swinging, the mD stride signature has a clear pronounced sinusoidal shape. This is particularly recognizable when the radar has a back view on the person. In this case, the salient spiky characteristic of a normal stride when walking away from the radar is absent as can be seen by comparing the first and second stride signature in (d).

The case when both legs cannot be bent properly is depicted in (e) and (f). We observe that the stride signatures for this walking style reveals smaller maximal Doppler shifts compared to a normal walk. In addition, the stride signatures do not show the typical clear sinusoidal shaped mD signatures for walking toward the radar. When the radar has a back-view on the person, the spiky behavior in the TFR, which is characteristic for a normal stride, is absent when the knee is not fully bent.

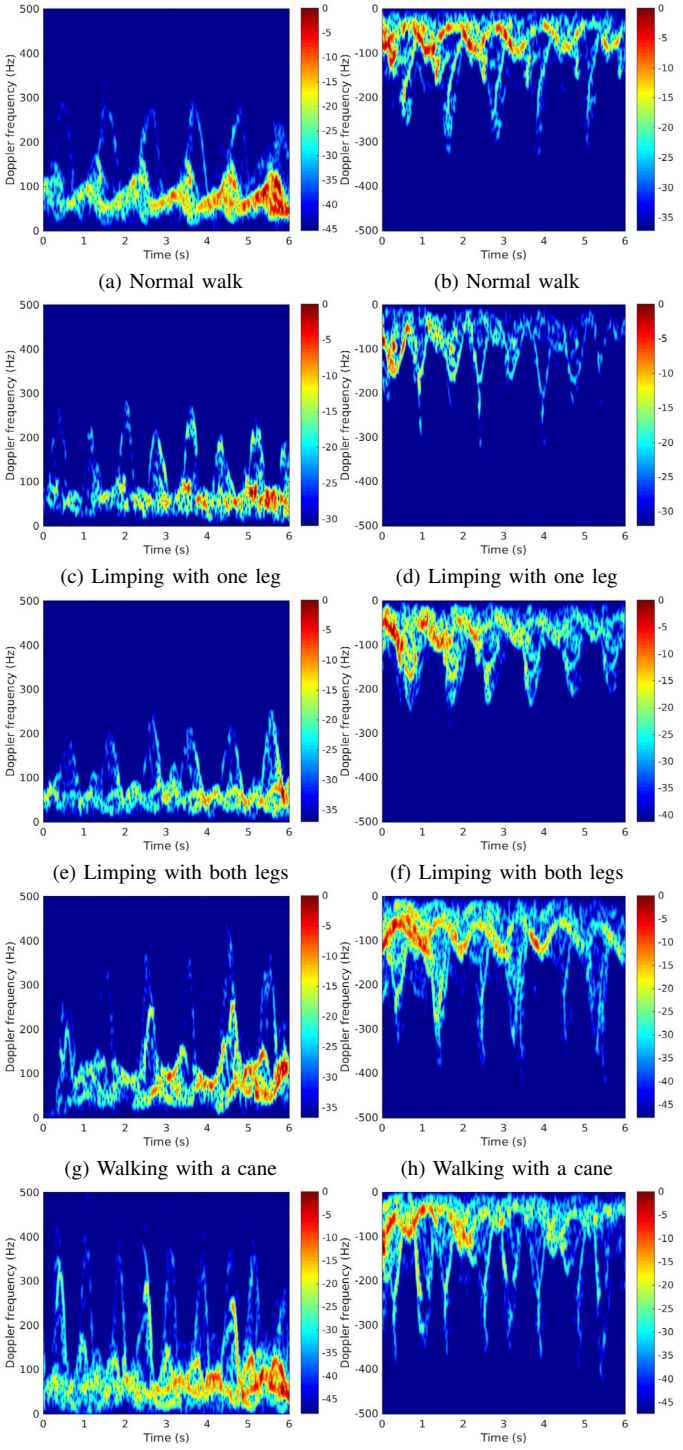

(a) Normal walk (b) Normal walk

(c) Limping with one leg (d) Limping with one leg

(e) Limping with both legs (f) Limping with both legs

(g) Walking with a cane (h) Walking with a cane

(i) Walking with a cane out of sync (j) Walking with a cane out of sync

Fig. 1: Examples of spectrograms for different human walking styles performed toward (left) and away from (right) the radar system.

The influence of using a cane on the mD signatures of a human walk is shown in (g) and (h) for toward and away from radar motions, respectively. In (g), the first, third and fifth stride signatures are altered by the cane's motion, i.e., leg and cane mD signatures are overlaying. Consequently, the energy of these mD signatures is higher compared to those of normal strides. In the case where the radar has a back view on the person, the spike behavior, which is characteristic of a normal stride, is eclipsed by the overlaying cane signature. This can be seen in the second, forth, and sixth stride signatures in (h).

In order to obtain isolated mD signatures of a swinging cane, (i) and (j) show the spectrogram of a person walking with a cane, where the cane is moved independently of both legs. The resulting mD signature sequence consists of an isolated cane signature followed by two stride signatures. This pattern is repeated three times during the measurement shown in (i). The away-from-radar measurement in (j) reveals the cane's signature at the second, fifth and eighth position.

III. Radar-based Gait Classification

A. Features from the Spectrogram

We calculate the spectrogram according to (1), where a Hamming window of length $L = 255$ and $K = 2048$ discrete frequency points is used, and $s(n)$ is the complex zero-mean radar return signal. In order to eliminate the Doppler signatures and obtain spectrograms as shown in Fig. 1, an adaptive thresholding technique is used to suppress the background noise in the TFR [27]. Next, we apply an energy-based thresholding algorithm for extracting the upper and lower envelopes for toward and away from radar motions, respectively [28]. An example of an envelope signal is given in Fig. 2(b). The absolute value of the envelope has minima during double support phases and maxima when a swinging foot or cane exhibits the maximal Doppler shift. Thus, we obtain a signal that lends itself to capture the inherent periodicity of the gait. Here, using the envelope has the advantage that it is not affected by the individual appearance or inherent pattern of the individual mD signatures in the time-frequency domain, but only represents the observed Doppler shift. Thus, all strides and even cane movements reveal a very similar shape in the envelope signal, which facilitates the estimation of the underlying gait periodicity.

For a normal human walk this periodicity relates to the stride rate, which is an important characteristic for describing a person's gait. However, for cane-assisted walks the stride rate may not be well defined: in the case where the cane is not moved synchronously with any leg, the strides become non-periodic, see e.g. Figs. 1(i) and 1(j). For this reason, we introduce the repetition frequency of mD signatures, f_{mD}, irrespective of being due to strides or cane movements. In order to obtain an estimate of f_{mD}, we calculate the Fourier transform (FT) of the extracted envelope and determine the maximum of its magnitude as indicated in Fig. 2(c) [29].

Since f_{mD} itself does not describe the considered walking styles appropriately, i.e., it is not a descriptive feature for gait recognition, we use it to define another feature: the gait harmonic frequency ratio [30]. It is calculated as the ratio between the FF estimate f_0 and the mD repetition frequency f_{mD}, i.e.,

$$\beta = \frac{f_0}{f_{\mathrm{mD}}}. \tag{2}$$

Here, we expect the values of β to be:

- 1 for normal walking and limping with both legs as each mD stride signature assumes the same pattern,
- $1/2$ for limping with one leg and walking with a cane in a synchronized manner as every other mD signature appears the same,
- $1/3$ for walking with a cane out of sync as a set of two strides and one cane movement constitutes one period.

In this paper, we find f_0 utilizing SOH modeling as described in the next section.

Further, we extract the maximal observed Doppler frequency $f_{\mathrm{D,max}}$ for each measurement as indicated in Fig. 2(a). Using again the envelope signal obtained from the noise-reduced spectrogram, we calculate the mean of the highest 10% of observed Doppler shifts [27]. In so doing, the maximal Doppler frequency estimate becomes less sensitive to outliers.

From the spectrograms in Fig. 1, we observe that some walking styles reveal different maximum Doppler shifts per leg motion. In particular, limping with one leg leads to a salient pattern of alternating high and low maximal Doppler frequencies, see Figs. 1(c) and 1(d). To capture this behavior, we use the peaks of the envelope signal and approximate the envelope's envelope using spline interpolation. In order to measure the variation in maximal Doppler shifts, we proceed to calculate the coefficient of variation given by

$$c_v = \frac{\sigma}{\mu}, \tag{3}$$

where σ is the standard deviation and μ is the mean of the interpolated signal.

B. Sum-of-Harmonics Modeling

The periodicity of the time-frequency signature along the time-variable can be revealed using non-parametric and parametric techniques. Whereas we use the former to identify the periodicity of mD signatures with time from the envelope signal, the latter models the behavior of the time-frequency signature as a SOH, and then proceeds to estimate the FF. In both cases, we obtain gait characteristics that, if put into relation, form a salient feature for gait classification, i.e., the feature β as given in (2).

To capture the characteristics of the different stride types, we define a signal $E(n)$ as

$$E(n) = \frac{1}{K'} \sum_{k=0}^{K'-1} \tilde{\mathrm{S}}(n,k), \quad n = 0, \ldots, N-1, \tag{4}$$

where $\tilde{\mathrm{S}}$ is the noise-reduced spectrogram, and $K' < K$ is the number of relevant frequency bins corresponding to the Doppler frequency range between an adaptive threshold and 500 Hz. Here, the threshold is chosen corresponding to $2v_0$, see Fig. 2(a), where v_0 is the average walking speed of the

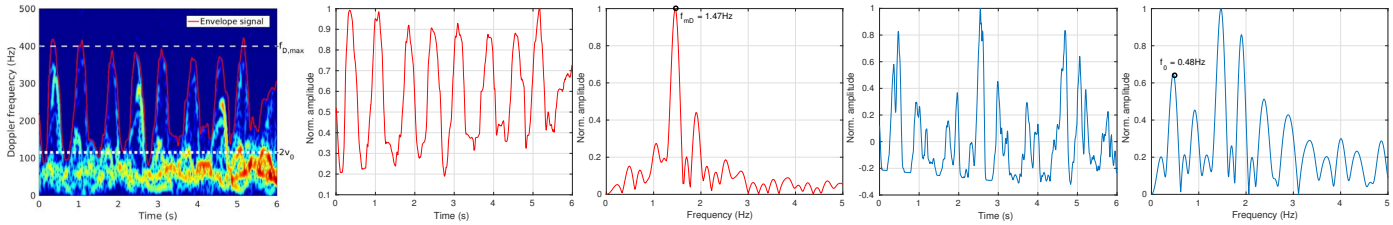

(a) (b) (c) (d) (e)

Fig. 2: (a) Spectrogram of a person walking with a cane out of sync. (b) Envelope signal of the mD signatures and (c) its FT with f_{mD} estimate. (d) The short-time energy signal $E(n)$ and (e) its FT with FF estimate f_0 obtained via SOH modeling.

person [23]. Adding the different Doppler frequency slices of the spectrogram above a specific frequency threshold, in essence, has the effect of summing up the signal power at high Doppler frequencies. This converts the time-frequency signal behavior into a signal composed of a train of pulses along the time variable, see Fig. 2(d). Thus, $E(n)$ can be interpreted as the short-time energy of the original radar return signal, where the background noise has been suppressed. The resulting signal reveals a periodic behavior along the time variable, which can be modeled as a SOH, i.e.,

$$\begin{aligned} x(n) &= \sum_{i=1}^{q} u_i \cos(2\pi i f_0 n) + v_i \sin(2\pi i f_0 n) \\ &= \sum_{i=1}^{q} \alpha_i \cos(2\pi i f_0 n + \phi_i), \end{aligned} \tag{5}$$

where f_0 is the FF in Hz, q is the number of harmonics (NOH), and the harmonic amplitudes and phases are α_i and ϕ_i, respectively. The ith harmonic frequency is given by if_0.

Given the signal $E(n)$, we use the algorithm proposed in [31] to estimate the FF, the NOH, and harmonic amplitudes and phases. For this, the measured data $E(n)$ is assumed to consist of a SOH signal $x(n)$ and an additive white Gaussian noise component $u(n)$, i.e.,

$$E(n) = x(n) + u(n), \quad n = 0, \ldots, N-1. \tag{6}$$

The parameters are found by minimizing the squared-error between the data and the model given by

$$\xi = \sum_{n=0}^{N-1} |x(n) - E(n)|^2 , \tag{7}$$

and utilizing the nonlinear least squares (NLS) method, for estimating f_0, augmented by a model order selection method, for detecting q. For this, (7) is jointly optimized over candidate FFs and candidate orders. Here, we use f_{mD} as an initial estimate of the FF. In a first step of the SOH algorithm, this estimate is refined by minimizing (7) using an optimization technique. Next, candidate FFs are determined from the refined f_0 estimate for which the cost function defined by the NLS method is evaluated. At this point, we incorporate prior knowledge to limit computational costs in the joint-optimization for finding f_0 and q, and avoid overfitting. As described in Section III-A, we expect the FF to be $1/3 \cdot f_{\text{mD}}$, $1/2 \cdot f_{\text{mD}}$ or $1 \cdot f_{\text{mD}}$ given the initial FF estimate f_{mD} is correct. Thus, the candidate FFs assume only the aforementioned values.

Given the estimates for f_0 and q, the SOH model in (5) is linear in the parameters u_i and v_i. Thus, using the linear least-squares solution, the harmonic amplitudes α_i and phases ϕ_i, $i = 1, \ldots, q$, can be computed in a closed-form as a function of f_0 and q. The estimated parameter vector is thus given by

$$\mathbf{p} = [f_0 \; q \; \alpha_1 \cdots \alpha_q \; \phi_1 \cdots \phi_q]^{\mathrm{T}} . \tag{8}$$

IV. Experimental Results

A. Experimental Setup

A 24 GHz UWB radar system [32] was used to collect experimental data in an office environment at Technische Universität Darmstadt, Germany. The antenna feed point was positioned approximately 1.15 m above the floor and four different test subjects were asked to walk back and forth between approximately 4.5 m and 1 m in front of the radar. All subjects were asked not to swing their arms. Data were collected with a non-oblique view to the targets and at a 0° angle relative to the radar line-of-sight. In total, 400 measurements of 6 s duration are considered including 200 toward and 200 away from radar motions. The number of data samples are equal among the test subjects and classes. We consider five different gaits: normal walking (NW), limping with one (L1) or both legs (L2), walking with a cane in a synchronized manner (CW) and out of sync (CW/oos). Thus, the data set contains 100 measurements per person and 20 samples per walking style.

B. Classification Results

The final feature vector, which is used for classification of different human walking styles, is defined as

$$\mathbf{z} = [f_{\text{mD}} \; \beta \; f_{\text{D,max}} \; c_v \; \alpha_1 \cdots \alpha_{q_{\max}}]^{\mathrm{T}} , \tag{9}$$

where $q_{\max} = 5$ is the maximal order of the SOH model and $\alpha_i = 0 \; \forall \; i > q$. The set of classes is defined as $\mathcal{C} = \{\text{NW}, \text{L1}, \text{L2}, \text{CW}, \text{CW/oos}\}$. Using 80% of the measurements we train a Nearest Neighbor (NN) classifier and evaluate its performance using the remaining 20% of data. All presented classifications rates are obtained by averaging over 500 classification results, where training and test samples are randomly chosen.

1) Gait harmonic feature: As described in Section III-A a descriptive feature for classifying different walking patterns is the gait harmonic frequency ratio β. Table I shows the results for classifying $\{\text{NW}, \text{L2}\}$, $\{\text{CW}, \text{L1}\}$ and CW/oos using only the aforementioned feature. Ignoring the direction of motion, (a) shows the confusion matrix for the three considered gait

TABLE I: Confusion matrices for classifying three different gait patterns using the gait harmonic feature β. Numbers represent the correct classification rates in %.

(a) both

True / Predicted	NW, L2	CW, L1	CW/oos
Normal walk (NW), Limping both (L2)	67	27	6
Cane - synchronized (CW), Limping one (L1)	18	77	5
Cane - out of sync (CW/oos)	5	1	94

(b) toward

True / Predicted	NW, L2	CW, L1	CW/oos
Normal walk (NW), Limping both (L2)	66	28	6
Cane - synchronized (CW), Limping one (L1)	12	79	9
Cane - out of sync (CW/oos)	9	3	88

(c) away

True / Predicted	NW, L2	CW, L1	CW/oos
Normal walk (NW), Limping both (L2)	68	27	5
Cane - synchronized (CW), Limping one (L1)	24	75	1
Cane - out of sync (CW/oos)	0	0	100

classes. In (b) and (c) the results for walking toward and away from the radar are given, respectively. We observe that the classification rates are higher, when the radar has a back view on the person, in particular for the class CW/oos. This is due to the very characteristic mD signature of a normal stride when observed from behind, which does not exhibit a sinusoidal shape in the TFR as a limping leg or a cane but a spiky behavior. Hence, in the sum over multiple Doppler frequencies, a normal stride leads to a short, impulsive-like waveform at intervals of $1/f_{\mathrm{mD}}$. This behavior leads to longer lasting harmonics in the spectrum compared to walking toward due to the impulsive-like waveform. Thus, the detection of sub-harmonics arising from gait abnormalities is facilitated.

2) Gait classification: Fig. 3 shows a scatter plot of the features f_{mD} and $f_{\mathrm{D,max}}$ for all persons. In this feature space, two gait classes are well separated: walking with a cane out of sync reveals the highest FF of all classes and limping with both legs typically reveals the smallest maximal Doppler shift. The former is due to the additional mD signature of the cane which leads to a higher mD repetition frequency, whereas the latter can be explained by the reduced redial velocity of a limping leg compared to a healthy foot swing.

The average correct classification rates for different persons as well as the whole data set are given in Table II. We can see that, in the person-specific scenarios, the presented approach achieves very high classifications rates, where the walks of persons A-D are correctly classified in 89%, 89%, 96% and 94% of the cases, respectively. For persons A and B the highest confusion appears among the classes NW and CW. In these cases, the cane was not correctly detected, but the gait was falsely classified as normal walking, which, in fact, is the underlying gait of walking with a cane.

The results for the person-generic case are given in Table II(d), where the entire data set, i.e., experimental data of all four persons, was used to train and test the classifier. The overall average classification accuracy decreases to 88%. Again, most of the confusion can be observed between the

TABLE II: Confusion matrices for classifying five different gait classes of four different persons. Numbers represent the correct classification rates in %.

(a) Person A

True / Predicted	NW	L1	L2	CW	CW/oos
Normal walk (NW)	70	4	4	21	1
Limping with one leg (L1)	4	95	0	1	0
Limping with both legs (L2)	0	0	100	0	0
Cane - synchronized (CW)	22	0	0	78	0
Cane - out of sync (CW/oos)	0	0	0	0	100

(b) Person B

True / Predicted	NW	L1	L2	CW	CW/oos
Normal walk (NW)	77	0	0	23	0
Limping with one leg (L1)	4	86	1	9	0
Limping with both legs (L2)	0	1	99	0	0
Cane - synchronized (CW)	16	3	0	81	0
Cane - out of sync (CW/oos)	0	0	0	0	100

(c) Person C

True / Predicted	NW	L1	L2	CW	CW/oos
Normal walk (NW)	100	0	0	0	0
Limping with one leg (L1)	4	95	0	0	1
Limping with both legs (L2)	0	0	92	6	2
Cane - synchronized (CW)	0	0	0	100	0
Cane - out of sync (CW/oos)	1	1	0	5	93

(d) Person D

True / Predicted	NW	L1	L2	CW	CW/oos
Normal walk (NW)	91	0	0	9	0
Limping with one leg (L1)	0	100	0	0	0
Limping with both legs (L2)	0	2	89	9	0
Cane - synchronized (CW)	5	1	1	93	0
Cane - out of sync (CW/oos)	2	0	0	0	98

(e) All

True / Predicted	NW	L1	L2	CW	CW/oos
Normal walk (NW)	82	0	4	14	0
Limping with one leg (L1)	1	90	3	5	1
Limping with both legs (L2)	4	3	90	3	0
Cane - synchronized (CW)	11	2	5	82	0
Cane - out of sync (CW/oos)	0	0	0	2	98

classes NW and CW, whereas CW/oos reveals the highest correct classification rate. Concluding, we note that in this case the person-specific training is advantageous over a person-generic one, which is evident from the higher individual classification rates.

V. Conclusion

The paper detailed the differences in radar mD signatures of different human walking styles. Considering normal, pathological and cane-assisted walks, physically interpretable features are extracted from TFRs incorporating SOH modeling to capture the underlying gait pattern. Experimental results verify that five gait classes can be correctly classified with high degree of reliability for different individuals. As such, this work furthers the understanding of radar-based gait analysis, which supports the idea of using radar as a diagnostic tool and thus paves the way for ambulatory medical gait analysis.

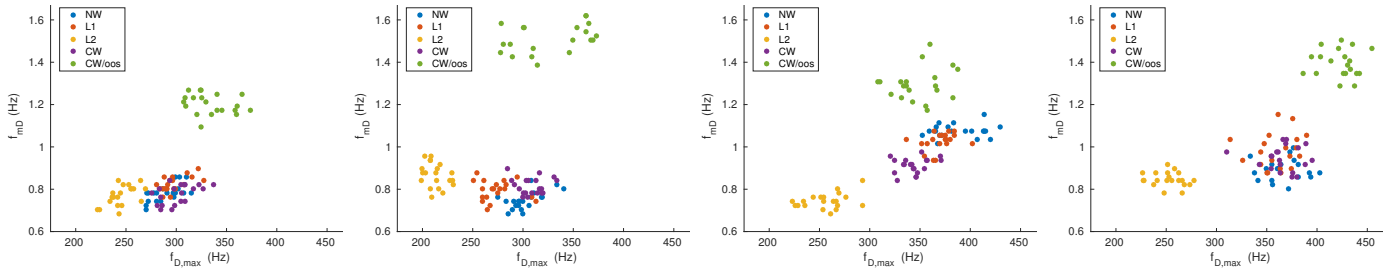

(a) Person A (b) Person B (c) Person C (d) Person D

Fig. 3: Scatter plots of the mD repetition frequency f_{mD} vs. the maximal observed Doppler shift $f_{\mathrm{D,max}}$ for different persons.

ACKNOWLEDGMENT

This work is supported by the Alexander von Humboldt Foundation.

REFERENCES

[1] M. W. Whittle, *Gait analysis: an introduction*, Butterworth-Heinemann, 2014.

[2] W. Pirker and R. Katzenschlager, "Gait disorders in adults and the elderly," *Wiener Klinische Wochenschrift*, vol. 129, no. 3-4, pp. 81–95, 2017.

[3] Stanford Medicine, "Gait abnormailies," http://stanfordmedicine25.stanford.edu/the25/gait.html, retrieved: 11/20/2017.

[4] M. G. Amin, Ed., *Radar for Indoor Monitoring: Detection, Classification, and Assessment*, CRC Press, 2017.

[5] V. C. Chen, D. Tahmoush, and W. J. Miceli, Eds., *Radar Micro-Doppler Signatures: Processing and Applications*, Institution of Engineering and Technology, 2014.

[6] S. R. Simon, "Quantification of human motion: gait analysis - benefits and limitations to its application to clinical problems," *J. of Biomechanics*, vol. 37, no. 12, pp. 1869 – 1880, 2004.

[7] A. Muro-de-la Herran, B. Garcia-Zapirain, and A. Mendez-Zorrilla, "Gait analysis methods: An overview of wearable and non-wearable systems, highlighting clinical applications," *Sensors*, vol. 14, no. 2, pp. 3362–3394, 2014.

[8] N. M. Gell, R. B. Wallace, A. Z. Lacroix, T. M. Mroz, and K. V. Patel, "Mobility device use in older adults and incidence of falls and worry about falling: Findings from the 2011–2012 national health and aging trends study," *J. of the Amer. Geriatrics Soc.*, vol. 63, no. 5, pp. 853–859, 2015.

[9] V. C. Chen, *The micro-Doppler effect in radar*, Artech House, 2011.

[10] M. Otero, "Application of a continuous wave radar for human gait recognition," in *SPIE Defense + Security*, 2005, pp. 538–548.

[11] I. Orović, S. Stanković, and M. Amin, "A new approach for classification of human gait based on time-frequency feature representations," *Signal Processing*, vol. 91, no. 6, pp. 1448–1456, 2011.

[12] F. Wang, M. Skubic, M. Rantz, and P. E. Cuddihy, "Quantitative gait measurement with pulse-Doppler radar for passive in-home gait assessment," *IEEE Trans. Biomed. Eng.*, vol. 61, no. 9, pp. 2434–2443, 2014.

[13] M. G. Amin, F. Ahmad, Y. D. Zhang, and B. Boashash, "Micro-Doppler characteristics of elderly gait patterns with walking aids," in *SPIE Defense + Security*, 2015, pp. 94611A–94611A.

[14] M. G. Amin, F. Ahmad, Y. D. Zhang, and B. Boashash, "Human gait recognition with cane assistive device using quadratic time-frequency distributions," *IET Radar, Sonar & Navigation*, vol. 9, no. 9, pp. 1224–1230, 2015.

[15] S. Z. Gurbuz, C. Clemente, A. Balleri, and J. J. Soraghan, "Micro-Doppler-based in-home aided and unaided walking recognition with multiple radar and sonar systems," *IET Radar, Sonar & Navigation*, vol. 11, no. 1, pp. 107–115, 2017.

[16] M. S. Seyfioglu, A. M. Özbaygglu, and S. Z. Gurbuz, "Deep convolutional autoencoder for radar-based classification of similar aided and unaided human activities," *IEEE Trans. on Aerosp. Electron. Syst.*, 2018, to be published.

[17] B. G. Mobasseri and M. G. Amin, "A time-frequency classifier for human gait recognition," in *SPIE Defense, Security, and Sensing*, 2009, pp. 730628–730628.

[18] F. H. C. Tivive, A. Bouzerdoum, and M. G. Amin, "A human gait classification method based on radar Doppler spectrograms," *EURASIP J. on Advances in Signal Process.*, vol. 2010, no. 1, pp. 389716, 2010.

[19] B. Lyonnet, C. Ioana, and M. G. Amin, "Human gait classification using microDoppler time-frequency signal representations," in *Proc. 2010 IEEE Radar Conf.*, 2010, pp. 915–919.

[20] F. H. C. Tivive, S. L. Phung, and A. Bouzerdoum, "Classification of micro-Doppler signatures of human motions using log-Gabor filters," *IET Radar, Sonar & Navigation*, vol. 9, no. 9, pp. 1188–1195, 2015.

[21] R. Ricci and A. Balleri, "Recognition of humans based on radar micro-Doppler shape spectrum features," *IET Radar, Sonar & Navigation*, vol. 9, no. 9, pp. 1216–1223, 2015.

[22] C. Clemente, L. Pallotta, A. D. Maio, J. J. Soraghan, and A. Farina, "A novel algorithm for radar classification based on Doppler characteristics exploiting orthogonal Pseudo-Zernike polynomials," *IEEE Trans. Aerosp. Electron. Syst.*, vol. 51, no. 1, pp. 417–430, 2015.

[23] A.-K. Seifert, A. M. Zoubir, and M. G. Amin, "Radar-based human gait recognition in cane-assisted walks," in *Proc. 2017 IEEE Radar Conf.*, 2017, pp. 1428–1433.

[24] A.-K. Seifert, M. G. Amin, and A. M. Zoubir, "New analysis of radar micro-Doppler gait signatures for rehabilitation and assisted living," in *Proc. 42nd IEEE Int. Conf. on Acoustics, Speech and Signal Processing (ICASSP)*, 2017, pp. 4004–4008.

[25] M. G. Amin, Y. D. Zhang, F. Ahmad, and K. C. D. Ho, "Radar signal processing for elderly fall detection: The future for in-home monitoring," *IEEE Signal Process. Mag.*, vol. 33, no. 2, pp. 71–80, 2016.

[26] A. V. Oppenheim, R. W. Schafer, and J. R. Buck, *Discrete-time Signal Processing*, Prentice-Hall, Inc., Upper Saddle River, NJ, USA, 1999.

[27] Y. Kim and H. Ling, "Human activity classification based on micro-Doppler signatures using a support vector machine," *IEEE Trans. Geosci. Remote Sens.*, vol. 47, no. 5, pp. 1328–1337, May 2009.

[28] B. Erol, M. G. Amin, F. Ahmad, and B. Boashash, "Radar fall detectors: a comparison," in *Proc. SPIE Defense + Security*, 2016, p. 982918.

[29] Y. Kim, S. Ha, and J. Kwon, "Human detection using Doppler radar based on physical characteristics of targets," *IEEE Geosci. Remote Sens. Lett.*, vol. 12, no. 2, pp. 289–293, Feb 2015.

[30] A. Alzogaiby, "Using micro-Doppler radar signals for human gait detection," M.S. thesis, Stellenbosch: Stellenbosch University, 2014.

[31] G. Whipps, "Coupled harmonics: estimation and detection," *Dissertation Ohio State University*, 2003.

[32] Ancortek Inc., "SDR-KIT 2500AD," http://ancortek.com/sdr-kit-2400ad, retrieved: 11/20/2017.